Lithium-Ion Batteries Containing Surfactants for the Protection of Graphite Anode against the Passivation Layer Byproducts

Fabien Chrétien,[a] Georgios Nikiforidis,[b] Christine Damas,[a] and Mérièm Anouti*[a]

The electrolyte is an essential component of all electrochemical devices, including lithium-ion batteries (LIBs). During the initial charging process, a portion of the electrolyte (usually a mixture of organic solvents and lithium salts) decomposes at the anode surface, forming a thin layer of solid electrolyte interface (SEI). This study examines the physicochemical properties of three surfactants: lithium dodecyl sulfate (LiDS), polyoxyethylene ether Forafac 1110D (LiF1110), and lithium perfluoro octanesulfonate Forafac 1185D (LiFOS). Initially, their thermal properties (surface tension and contact angle) are determined. Then, electrochemical tests (cyclic voltammetry, galvanostatic charge-discharge cycling, and electrochemical impedance spectroscopy) followed by ex-situ X-ray photoelectron spectroscopy (XPS) measurements on the graphite anodes in a standard

electrolyte ethylene carbonate/propylene carbonate/3 dimethyl carbonate $+1\,mol\,L^{-1}$ $LiPF_6$ are conducted to compare the surfactants' action according to their chemical structure, as well as their effect on the interface properties of the formed SEI. The results indicate that surfactants improve electrode interfaces due to their amphiphilic character, preventing the harmful effects of passivation layer salts (LiF, LiOH, Li2O, etc.) that deposit on the graphite interfaces. The three surfactants affect the cycling behavior and performance of the half-cells differently depending on their ionic or nonionic nature and the polarity or non-polarity of the salt (e.g., lithium fluoride LiF, lithium oxide Li_2O), with LiF1110 demonstrating the best performance.

Introduction

Lithium-ion batteries (LIBs) have been widely used in electronic devices for many decades and are currently making their way into the energy storage market (i.e., they are one of the dominant storage technologies for large-scale plants to help electricity grids ensure a reliable supply of renewable energy) as well as the electrification of transportation. On top of their flexibility and falling prices, advances in digital technologies such as artificial intelligence, blockchain, and predictive analytics are spurring innovative storage business models. Meanwhile, a great deal of research on the (electro)chemistry and operating performance characteristics (primarily the energy density) of LIBs is currently underway.

In a nutshell, LIBs are typically based on a graphite negative electrode (with a theoretical specific capacity of $372\,mAh\,g^{-1}$, anode)[1] and a lithium transition metal oxide positive electrode

(cathode).[2] Commonly used linear or cyclic alkyl carbonates (that decrease the melting point and viscosity such as ethylene carbonate, dimethyl carbonate, ethyl methyl carbonate) dissolved in the appropriate lithium-based salt (i.e., lithium hexafluorophosphate, $LiPF_6$) are electrochemically reduced at the anode surface during the initial cycles forming an insoluble passivating film known as the solid-electrolyte interphase (SEI).[3] The latter is a critical component of LIBs in that it prevents further electrolyte or solvent decomposition (i.e., SEI hinders electron tunnelling from the electrode[4]), facilitates the Li^+ transport and adds stability and durability to the cell, namely the power capability, safety, and cycle life. It is well accepted today that the SEI is ≈ 10–$50\,nm$ thick and comprises inorganic salts (e.g., Li_2CO_3, Li_2O, LiOH and LiF)[5] along with decomposed carbonate molecules.[6] These species are usually arranged in stratified structures, with the innermost layer being more inorganic (i.e., LiF and Li_2O) and the outer layer more organic (e.g., semi-carbonates, oxalates, alkoxides, and polymers).[7] Hence, their precipitation and accumulation at the interfaces (e.g., graphite, lithium metal, separator), and their suspension in the electrolyte due to small crystallite size[8] can be either beneficial or detrimental. More precisely, certain SEI components such as Li_2CO_3 and LiF have been reported to enhance the quality of the passivation layer[9] while others (Li_2O, LiOH) are harmful since they accentuate the insulating character of the SEI.[10] Given the significance and fragility of the SEI layer (the solubility of the above salts depends on the nature of the formed salt and the solvent mixture used), additives are widely used as a means to regulate their characteristics and improve the performance and safety of the battery.

[a] Dr. F. Chrétien, Dr. C. Damas, Prof. M. Anouti
Laboratoire PCM2E,
Université de Tours,
Parc de Grandmont, 37200 Tours, France
E-mail: meriem.anouti@univ-tours.fr

[b] Dr. G. Nikiforidis
Institute for Materials Discovery,
University College London,
Malet Place, WC1E 7JE London, UK

ChemElectroChem

Research Article
doi.org/10.1002/celc.202300102

**Chemistry
Europe**
European Chemical
Societies Publishing

The electrolyte properties dictate how fast the cell reaction can proceed (i.e., power density) and how many times a battery can be charged and discharged (cyclability).[7,11] Additives are an essential electrolyte component along with salt and solvent.[12] The ideal amount of the selected additive likely depends on its function in the cell and the amount needed to obtain the desired effect (especially at the interface of electrode/electrolyte) without having a significant negative influence on other properties impacting the performance.[6] Amongst the various classes of additives used,[13] surfactants owing to their specific spatial organization[14] emerge as promising candidates to alleviate the interfacial interactions that stem from the SEI layer formation.[15]

Herein, we oriented the scope of the role of surfactants as protectors/stabilizers of the SEI in the presence or absence of (mineral) salts comprising the SEI (i.e., LiF, LiOH, Li_2CO_3, Li_2O). The following three surfactants have been selected, namely, lithium dodecyl sulfate (LiDS), polyoxyethylene ether Forafac 1110D (LiF1110), and lithium perfluoro octanesulfonate Forafac 1185D (LiFOS). The perfluorinated LiFOS and LiF1110 are products of the company DuPont marketed under the name Forafac.[16] The aforementioned surfactants (Table 1) are selected on account of their (i) polar or apolar character (e.g., ionic or non-ionic surfactant), (ii) hydrophobicity and interfacial properties (hydrophobic C–H or C–F bonds), and (iii) complexxation ability owing to the ether function C–O–C.[17]
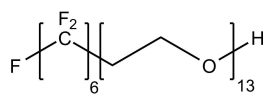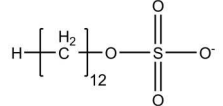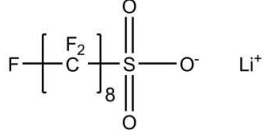
LiDS is a lithium anionic surfactant similar to sodium dodecyl benzene sulfate (NaDS),[18] that has been widely used in aqueous solutions (primarily due to its low cost).[19] It has been successfully integrated as a functional Li salt for aqueous LIBs with moderate performance[20] while its NaDS has been reported to accelerate the Li-ion diffusion at the LFP (lithium iron phosphate) electrode on an LFP//zinc cell.[19] To our knowledge, LiDS has not been studied in an organic environment (i.e., the presence of hydrocarbon chains in the LiDS structure makes it poorly soluble in organic solvents). LiFOS (a highly fluorinated anionic surfactant) has been used as an additive in lithium anodes in blended solutions comprising propylene carbonate (PC), ethylene carbonate (EC) and 1,2 dimethoxyethane (DME) and lithium perchlorate ($LiClO_4$).[16] The addition of this surfactant (the perfluorinated chains render it highly soluble to organic solvents) enhanced the lithium

anode cyclability due to (i) a less porous structure restricting the exposure of the Li surface to a chemical attack by the solvent; (ii) larger dendrites or particles of Li leading to reduced intergranular corrosion, and (iii) greater nucleation density leading to a uniform distribution of the Li particles. Dai et al.[14a] found that the addition of hexadecyl trimethylammonium chloride (CTAC, a cationic surfactant) as an additive in the PC-EC-dimethyl carbonate (DMC)-$LiPF_6$ electrolyte can aggregate the protuberances of lithium deposition via electrostatic attraction and suppress the growth of lithium dendrites by lithiophobic repulsion mechanisms. Besides, another cationic additive, heptafluorobutyric (HFA) in the presence of EC/DMC was found to optimize the Li-ion solvation for stable Li and zinc plating/stripping; the presence of long fluorinated chains facilitates the formation of a uniform inorganic SEI and a compact electrolyte interface while also enhances the wettability of the separator.[21]

Moreover, LiFOS has been implemented in high-capacity lithium-oxygen batteries as a perfluoro-surfactant and supporting electrolyte, which allowed exceptionally high miscibility of perfluorochemicals with tetraethylene glycol dimethyl ether (TEGDME) and an improved electrochemical reduction current of oxygen.[22] F1110D[23] is a non-ionic surfactant which contains oxyethylene units in a similar fashion to glymes (i.e., a long-chain glyme ending in a perfluorinated carbon chain of six carbons, Table 1) and has been used as an additive in acid-based zinc cells[23] and LiS batteries[24] where the micelle structure of the amphiphilic surfactant prohibits polysulfide formation. In literature, the addition of surfactants as additives to improve advanced battery interface (LiS, Zinc and aqueous LIBs), is certainly recognized as a promising approach as mentioned above, but no clear mechanism or comparison between surfactant classes (ionic, non-ionic, fluorinated or not, oxygenated or not) is discussed. Surprisingly, few to no works to our knowledge report the effect of surfactants on graphite as an anode, even though it is widely used in Li-ion batteries and its surface is highly sensitive to cycling due to the formation of the SEI.

In this study, the physicochemical properties of the selected surfactants, together with their thermal properties such as surface tension and contact angle, are initially analyzed. Next, electrochemical tests including cyclic voltammetry, galvano-

Table 1. Chemical structure and properties of the surfactants investigated in this study; LiDS, LiFOS and LiF1110. MW denotes molecular weight, T_f stands for melting temperature, S denotes the maximum solubility in ternary mixture EC/PC/3DMC and C represents the concentration of the additives.

	F1110D	LiDS	LiFOS
Chemical structure			
Formula	CF_3–$(CF_2)6$–$(C_2H_4O)_{12}H$	$C_{12}H_{25}OSO_3Li$	$F(CF_2)_8SO_3Li$
MW [g mol^{-1}]	892.7	272.3	506.1
T_f [°C]	$-8^{[a]}$	138	$338^{[a]}$
S [mol dm^{-3}]	> 0.1	$3.47 \times 10^{-5[b]}$	> 0.1
C [mol dm^{-3}]	2.5×10^{-3}	$> 3.47 \times 10^{-5}$ (saturated)	2.5×10^{-3}

[a] Values from ARKEMA, verified by differential scanning calorimetry analysis. [b] Solubility limit by atomic absorption spectroscopy (Figure S1).

static charge-discharge cycling, and electrochemical impedance spectroscopy are conducted. Ex-situ X-ray photoelectron spectroscopy (XPS) measurements are also performed on graphite anodes in a ternary carbonate mixture comprising PC, EC, and DMC. Herein, we examine the effect of these surfactants as additives in the standard electrolyte commonly used in industrial batteries[25] and widely used as an optimized electrolyte formulation for Li-ion batteries in the literature[5a,26] i.e., (EC/PC/3DMC, by weight) with 1 mol L^{-1} lithium hexafluorophosphate salt (LiPF$_6$), on the interfacial properties and performance of LIBs.

Results and Discussion

Physicochemical characterisation

F1110D can be described as a long-chain glyme, and BASF has reported that their high glymes are soluble in all proportions into several organic solvents such as diethyl ether and octane. The LiDS behavior is not well-documented in non-aqueous solutions, particularly its solubility, which is believed to be poorly soluble in organic electrolytes such as PC, EC and DMC. Tadano[27] used LiDS in N-methylpyrrolidone at a concentration of ca. 4×10^{-3} mol dm^{-3} while solubilities of LiDS and LiFOS in PC have been reported to be less than 2.5×10^{-4} and 0.12 mol dm^{-3}. Besides, in a PC/EC/2DME (1:1:2 %v) solution, the solubility of LiDS reached 4.7×10^{-3} mol dm^{-3} and for LiFOS 1.67 mol dm^{-3}.[16] Here, LiDS is introduced at saturation, attaining a concentration of 2.68×10^{-4} mol dm^{-3}. With the above in mind, the solubilities of LiFOS and F1110D are identical and based on the previous scarce literature while the LiDS concentration is determined by atomic absorption spectroscopy.

The thermal behavior of the surfactants in Table 1 (within -60 and $150\,°C$) is shown in Figure 1a. The heat flux is expressed in mW mg^{-1} to level the mass differences between the samples. F1110D exhibits a cold crystallisation at $-10.3\,°C$, during heating. Upon cooling, a phase change between 0 and $40\,°C$ is evident, indicative of a crystal-type liquid, bound to its amphiphilic bi-block structure.[24] Concerning the LiDS, during the first cycle, it shows an endothermic peak at $137.6\,°C$, in line with its melting temperature (Table 1). Since the differential scanning calorimetry (DSC) capsules are perforated to avoid any increase in pressure, it is assumed that LiDS is hydrated (i.e., the perforation leads to the sample(s) being in contact with air). The second cycle displays an endothermic peak at $14.2\,°C$ and a reversible exothermic one at $8.8\,°C$, attributed to the phase change of the liquid phase compound (i.e., strong organization). LiFOS remains stable over the selected measurement range and does not reveal any peaks. Overall, the investigated compounds are thermally stable up to $150\,°C$ and therefore suitable for use in carbonate-based electrolytes for LIBs. It should be noted that the phase changes observed in solvent-free additives are unlikely to occur when they are present in the ternary carbonate mixture. This is because the additives will be
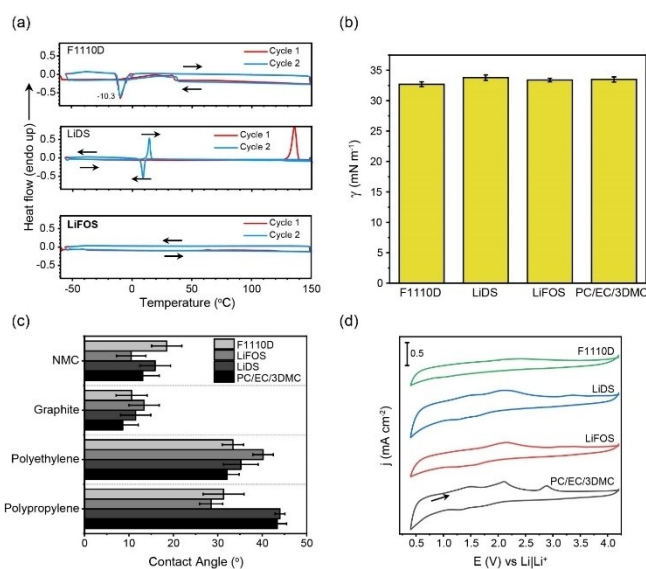

Figure 1. (a) Thermograms of the three different additives mixtures investigated in this study. (b) Surface tension of the additives obtained in PC/EC/3DMC by the Du Noüy ring method.[22] (c) Static contact angle of a PC/EC/3DMC solution with or without the surfactants on different surfaces at 25 °C. NMC stands for nickel manganese cobalt (522). (d) Electrochemical window of the electrolytes listed above. The supporting salt is 1 mol dm^{-3} LiPF$_6$. The cyclic voltammetry was conducted on lithium/platinum electrodes at 25 °C. The results of the second cycle are shown here. The arrow denotes the direction of the voltammogram. The scan rate is 50 μV s^{-1}.

solvated by the carbonates, which will lead to a different molecular organization.

The surface tension (γ) associated with the cohesive forces within the electrolytes studied (i.e., PC/EC/3DMC with and without the presence of the additives, Figure 1b) is sensitive to surface changes. The γ values of the carbonate mixture reach 33.5 mN m^{-1} while the addition of surfactants leads to a negligible variation, between 0.8 and 0.3 mN m^{-1}. The perfluorocarbon additives exhibit mild surface activity due to the hydrophobic and lipophobic character of the fluorocarbon chains. The wettability (i.e., the ability of a liquid to spread over a solid surface) of the electrolytes is measured through the contact angle (θ, Figure 1c) on different surfaces, namely polyethylene (PE), polypropylene (PP) (i.e., base materials comprising the separators), graphite and NMC ($=$Ni$_x$Co$_y$Mn$_z$O$_2$ is the formula of metal transition oxide cathode abrevied NMC in battery domain (nickel cobalt manganese)). For the last two, there is no significant enhancement in the wettability when the additives are present with θ lying between 8 and 20° (i.e., high surface energy). It should also be noted that these measurements show a large margin of error due to their porous nature which accentuates the spreading of the drop and decreases the measured contact angle. On the contrary, the wettability of polypropylene and polyethylene is higher, lingering between 30 and 40°. Adding LiFOS or F1110D improves the wettability of polypropylene (e.g., 44° to 28.5° for LiFOS) as opposed to polyethylene.

After validating the surfactants' inert thermal behavior and absence of surface activity in the presence of the ternary

carbonate mixture, their electrochemical behavior was investigated by cyclic voltammetry on lithium/platinum electrodes (Figure 1d). The electrochemical window of the platinum working electrode in the presence of the surfactants within a voltage range of 3.75 V (i.e., 0.4 to 4.15 V vs. Li/Li$^+$) is in line with typical carbonate electrolytes used in LIBs.[28] There is no indication of any reaction(s) that could manifest in the form of an irreversible peak or abrupt current increase, within this voltage range (i.e., the surface activity is not manifested by parasitic redox reactions). This is expected given the low amount (w%) of the surfactant(s) in the mixture, yet it is essential to validate the inertness of the working electrode surface.

Electrochemical characterisation

Figure 2 shows the voltammetry curves (CV) of graphite anodes during the first cycle in the presence of the surfactants exempting the lithium insertion domain (i.e., < 0.4 V vs. Li/Li+). In this voltage range, we can observe the formation of the passivation layer (SEI) during the first cycle and other reaction(s) that can take place in the presence of the surfactant(s) on the graphite surface. The low potential region (i.e., 0.4–1.0 V vs. Li/Li+) of the CV denotes the SEI layer formation.[29] A shoulder is evident around 0.9 V vs. Li/Li+ for all electrolytes, followed by a pronounced peak assigned to the irreversible decomposition of electrolyte (initiated by the EC polymerization) and SEI formation as described largely in literature.[30] The potential of this peak (between 0.69 and 0.71 V vs. Li/Li+) is not influenced by the presence or the nature of the surfactant. A non-pronounced carbonate reduction peak (i.e., indicative of good reduction stability) suggests a suppressed electrolyte decomposition reaction. The broad peak at 2.25 V vs. Li/Li+ for the PC/EC/3DMC/LiPF6/LiDS electrolyte is due to (water) impurities trapped on the micellar structure of the surfactant. Overall, in the presence of the surfactants, the studied electrolytes form a stable SEI layer and show no evidence of oxidative reaction(s) to voltages up to 4.2 V vs. Li/Li+ (Figure 2b).

In the case of the reference electrolyte (PC/EC/3DMC), 1 mol dm^{-3} LiPF$_6$ and LiDS, there is an upward (exponential) rise in current with higher cell voltages. In the presence of the LiFOS and F1110D surfactants, there is a small/negligible oxidation peak around 4.2 V (more pronounced in the case of LiFOS), probably due to fluorine degradation stemming from the oxidative environment.[31] Pierpaoli et al. proposed the electrochemical anodic degradation mechanism of polyfluorinated alkanes via Kolbe reactions with the elimination of two fluoride ions resulting from consecutive radical reactions.[31] In all cases, the intensity of the peak remained limited and only occurs beyond 4.0 V (essentially for LiFOS). Figure 3 shows the reversible intercalation/deintercalation peaks[32] (i.e., the pairs of peaks A–A', D–D' and E–E') for the first and seventh cyclic voltammograms between 0 and 0.25 V vs. Li/Li+ for all solutions. Peak D (0.075 V vs. Li/Li$^+$) denotes the first step of insertion of lithium (i.e., Li$_{0.2}$C6→Li$_{0.5}$C$_6$) where one space out of two between two graphene planes is filled with Li. Peak E (0.025 V vs. Li/Li$^+$) signifies the completion of Li$_{0.5}$C$_6$ to LiC$_6$.[5a] Points B and C describe the intermediate stages of the insertion mechanism. Upon the reversal of the scan direction, the deintercalation peaks (A', D' and E') are evident. They exhibit, however, different reversibility, i.e., $\Delta E_{E/E'} = 100$ mV $= \Delta E_{D/D'}$ while $\Delta E_{A/A'}$ is equal to 48 mV. Beyond 0.25 V no reaction is present, ensuring the absence of secondary reaction(s) of the material or electrolyte within this cell operating range.

The addition of LiDS increases the reduction potential (0.119 to 0.125 V) and reduces the oxidation potential (0.067 to 0.086 V) with an increasing number of cycles. The reduction and oxidation peaks are better defined (viz. reversible) at the 7th cycle indicating an easier intercalation-deintercalation mechanism into the graphite layers and hinting at the formation of an effective SEI on the graphite surface in this solution. For the cases of F1110D and LiFOS, both voltammograms reveal similar behavior to the reference electrode. Peak E in the F1110D and
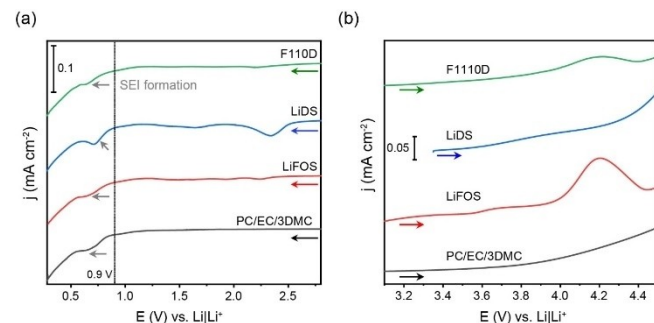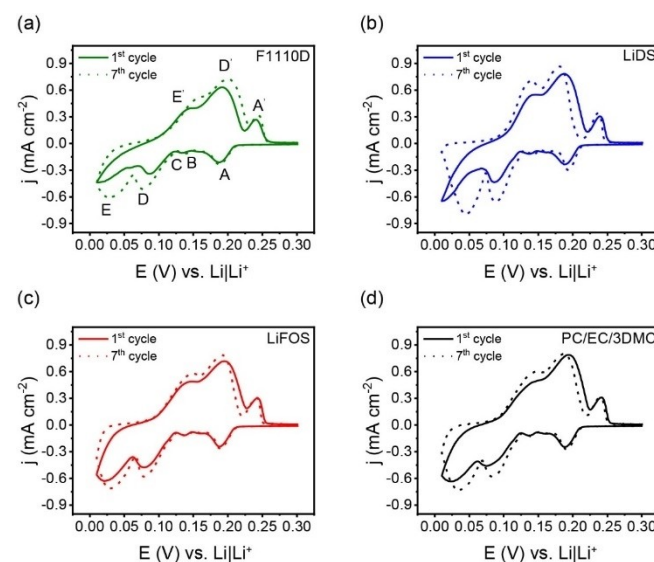
Figure 2. Negative (a) and positive (b) sweep voltammograms of the first cycle of three-electrode cells having graphite anodes and lithium metal as a reference and counter electrode in the presence of the electrolytes listed in Table 1. The scan rate is 50 µV s^{-1}. The arrows denote the direction of the voltammograms. The operating temperature is 25 °C.

Figure 3. First and seventh cyclic voltammetry plot of a Li-graphite cell under a standard carbonate electrolyte (PC/EC/3DMC), 1 mol dm^{-3} LiPF$_6$, and different surfactants (a) F1110D, (b) LiDS, (c) LiFOS, (d) without surfactant. The concentration of the surfactants is given in Table 1. The scan rate is 5 µV s^{-1}. The operating temperature is 25 °C.

ChemElectroChem

Research Article
doi.org/10.1002/celc.202300102

Chemistry
Europe
European Chemical
Societies Publishing

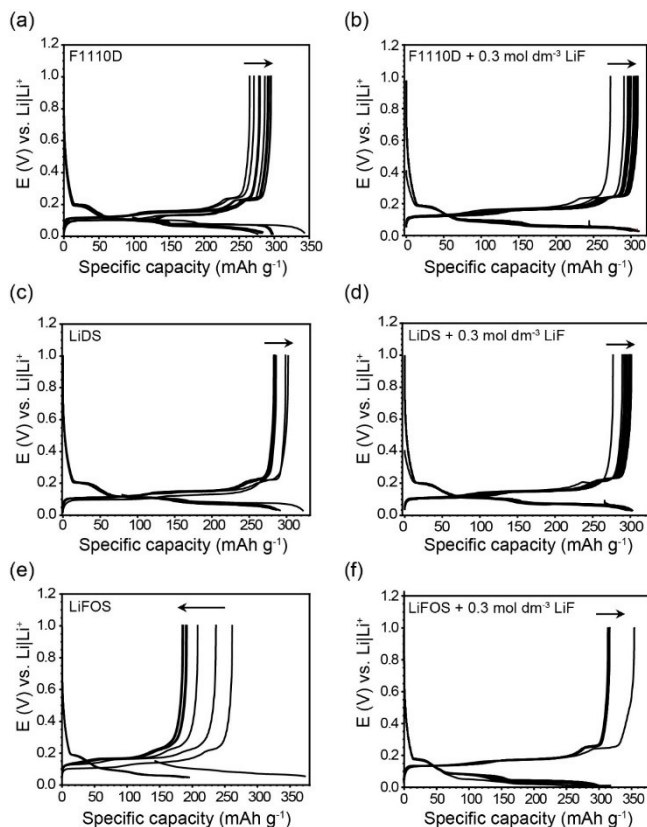**Figure 4.** Voltage profiles of Li/graphite coin cells under different surfactants in PC/EC/3DMC and 1 mol dm^{-3} LiPF$_6$ with and without LiF at room temperature and a C/10 rate. (a) F110D, (b) F110D + 0.3 mol dm^{-3} LiF, (c) LiDS, (d) LiDS + 0.3 mol dm^{-3} LiF, (e) LiFOS, (f) LiFOS + 0.3 mol dm^{-3} LiF.

LiFOS-based electrolytes was smaller than that in the standard electrolyte implying a mitigated Li$^+$ insertion rate in the graphite electrode at this voltage. Overall, at this intermediate charge/discharge rate, the Li$^+$ ions intercalate into graphite in the presence of the additives as effectively as in the standard ternary carbonate electrolyte.

The composition of the SEI layer has been reported to comprise different salts such as LiF, Li$_2$CO$_3$, LiOH, Li$_2$O, LiOCH$_3$ and LiOC$_2$H$_5$.[33] While Li$_2$CO$_3$ and LiOCH$_3$ are beneficial when added as additives in the electrolytes,[5a] LiOH and Li$_2$O have been found to disrupt the operation of both the graphite anode and lithium metal.[5a] LiF is concentration dependent; above 0.1 mol dm^{-3} it hampers the SEI fragility in the ternary mixture *PC/EC/3DMC*.[5a] With the above in mind, LiF (0.3 mol dm^{-3}), LiOH (3.0×10^{-3} mol dm^{-3}) and Li$_2$O (3.0×10^{-3} mol dm^{-3}) are being added to the existing electrolytes and their cycling behavior on graphite is evaluated (Figure 4) and summarized as a function cycle number at Figure 5. The concentration of these salts is based on their solubility in alkyl carbonates.[8b,34]

The addition of the LiDS and F1110D on the ternary electrolyte does not alter the typical profile for a Li-graphite half-cell where an irreversible capacity of the first charge/discharge cycle ($\approx$16%), corresponding to the formation of the SEI is evident (Figures 4a and 4c). On the other hand, the cell containing LiFOS (Figure 4e), exhibits a highly irreversible first cycle (32%) along with an incomplete third plateau, signifying a high lithium surface resistance. In all cases, the addition of LiF (at saturation→0.3 mol dm^{-3}, Figures 4c, 4d, and 4f) reveals an improvement in the discharge profiles together with high-capacity retention and coulombic efficiency for a total of 15 deep cycles, as seen in Figure 5. It should be noted that high amounts of LiF hinder the SEI formation on the graphite and in

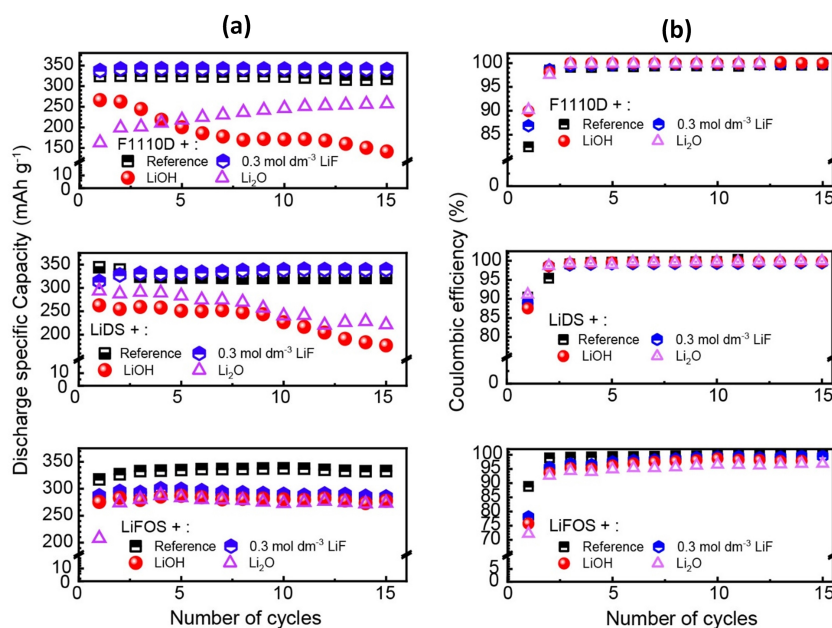**Figure 5.** Discharge specific capacity (a) and coulombic efficiency (b) of graphite-Li half-cells in PC/EC/3DMC, 1 mol dm^{-3} LiPF$_6$ and the surfactants of Table 1, namely LiDS (at saturation), 2.5×10^{-3} mol dm^{-3} F1110D and 2.5×10^{-3} mol dm^{-3} LiFOS. Furthermore, as a comparison 0.3 mol dm^{-3} LiF, Li$_2$O (3.33×10^{-4} mol dm^{-3}) and LiOH (3×10^{-3} mol dm^{-3}) are added for comparison purposes. The current rate is C/10 and the operating temperature 25 °C.

turn the specific capacity of the cell[9b,35] but in the presence of the surfactants that is not the case.

For comparison purposes, Figure 5 shows the performance of Li-graphite cells with electrolytes comprising the ternary carbonate electrolyte, the surfactant as well as the inorganic compounds LiOH (3.0×10^{-3} mol dm^{-3}) and Li$_2$O (at saturation, i.e., 3.0×10^{-3} mol dm^{-3}). The above inorganic products comprise the inner SEI layer next to the graphite while the outer one is composed of organic compounds such as ROLi and ROCO$_2$Li.[36] The performance characteristics of the cell containing F1110D indicate that only LiF is fit for long-term performance. The presence of LiOH hammers the discharge capacity (i.e., 160 mAh g^{-1} at cycle 10).

Then again, Li$_2$O generates a low capacity during the first cycles, which increases later on and stabilizes around 255 mAh g^{-1} after 15 full cycles. Regarding the LiDS, the discharge specific capacity reaches initially 350 mAh g^{-1} on par with the theoretical capacity of graphite under various electrolyte formulations.[28] The performance of the cell under this electrolyte stabilizes at 325 mAh g^{-1} throughout the cycling protocol. With prolonged cycling, the cells show a considerable capacity decrease (between 42 and 50%) in the presence of Li$_2$O and LiOH (Figure 5, Table 2). On the contrary, the simultaneous presence of LiF enhances and stabilizes the capacity (339 mAh g^{-1} at the 15th cycle) at a C/10 rate, which is markedly higher when compared to the same electrolyte in the absence of LiDS (i.e., 247 mAh g^{-1} at the 15th cycle, Table 2), indicating a favorable interaction between these compounds. The coulombic efficiencies obtained are high and attain 99% from the third cycle (Figure 5), irrespective of the SEI-related component added. It should be noted that the low efficiency in the first cycle stems from the SEI formation.[11]

For the case of LiFOS, the initial specific capacity is lower than the other two additives (344, 325 vs. 317 mAh g^{-1}, Table 2) and marginally higher than the standard electrolyte (330 vs. 338 mAh g^{-1} at cycle 15, Table 2). In the presence of the three SEI-related salts, the capacities are close to each other, lingering between 275 and 280 mAh g^{-1}, lower than the other inves-

tigated additives as are the coulombic efficiencies (e.g., LiFOS in the presence of LiOH or Li$_2$O achieve coulombic efficiencies of 98.65 and 96.54%, respectively). Yet, the specific capacities obtained for the electrolytes containing the Li$_2$O and LiOH (≈ 280 mAh g^{-1}) at the end of the cycling protocol were the highest amongst all values, highlighting the somewhat inhibiting nature of LiFOS towards the SEI components.
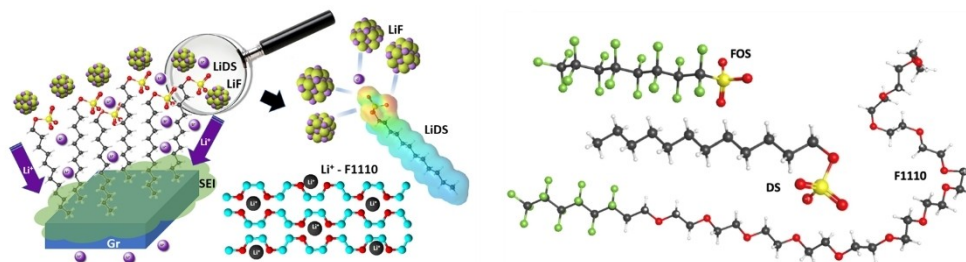
The half-cell results imply that the effect of surfactants is inseparable from the nature of the added salt. The interaction of ionic surfactants (LiDS and LiFOS) differs from the one of the non-ionic F1110D. The glyme functions of the latter are not unrelated to the complexation of free Li$^+$ or bound lithium cations (that are present in LiF, LiOH and Li$_2$O salts); the perfluorinated chain protects the formation of a passivation layer against a deposit of sparingly soluble salts as exemplified in the Scheme 1 below.

XPS and EIS analysis of the graphite surface

The effect of the simultaneous presence of the surfactants and LiF on the SEI formed on the graphite surface at a de-lithiated stage (i.e., the end of their cycling protocol) is investigated through XPS. The oxidation state and chemical bonding of carbon, along with oxygen, nitrogen, fluorine, and lithium (e.g., C 1s, F 1s, P 2p, O 1s and Li 1s) are illustrated in Figure 6. The C 1s peak in the spectra corresponds to the binding energy of the electrons in the carbon atoms of the graphite. The shape and intensity of the peak can provide information about the chemical bonding and crystal structure of the graphite, as well as any surface contaminants or defects. In this case, the spectrum of the graphite samples presented four deconvolution peaks, corresponding to the C=C/C–C in aromatic rings (graphite, 284.5 eV), epoxy C (C–O, 286.8 eV), carbonyl C (C=O, 287.8 eV) and carboxyl C (–COOH, 289.0 eV)[37] with no noticeable differences when compared to the reference electrolyte. The presence of LiDS, F1110D and LiF do not alter the structure of the graphitic material.

Table 2. Discharge specific capacities and coulombic efficiency of cycles 1 and 15 at a graphite-lithium half-cell. The current rate is C/10. The operating temperature is 25 °C. The electrolytes comprise a PC/EC/3DMC (%w) mixture with 1 mol dm^{-3} LiPF$_6$, LiDS (at saturation), 2.5×10^{-3} mol dm^{-3} F1110D, 2.5×10^{-3} mol dm^{-3} LiFOS, 0.3 mol dm^{-3} LiF, LiOH (at saturation) and 3.33×10^{-4} mol dm^{-3} Li$_2$O (at saturation).

Reference: EC/PC/3DMC + 1 mol dm^{-3} LiPF$_6$		Discharge specific capacity [mAh g^{-1}]		Coulombic efficiency [%]	
		1st cycle	15th cycle	1st cycle	15th cycle
Reference[5a]		303	330	93.6	99.7
Ref+	LiF	337	247	87.1	99.7
	LiOH	285	254	74.5	99.7
	Li$_2$O	273	252	71.9	99.8
Ref+LiDS		344	322	90.5	99.8
Ref+LiDS+	LiF	314	339	88.8	99.3
	LiOH	263	227	87.5	99.8
	Li$_2$O	294	240	91.1	99.8
Ref+LiFOS		317	338	88.8	99.7
Ref+LiFOS+	LiF	275	279	78.1	99.3
	LiOH	276	280	75.7	98.6
	Li$_2$O	208	273	72.1	96.5
Reference+F1110D		325	323	82.4	99.4
Ref+F1110D+	LiF	338	341	86.9	99.8
	LiOH	266	171	89.9	99.9
	Li$_2$O	163	246	90.2	99.9

Scheme 1. LiDS and LiFOS prevent polar salts (LiF) to reach the SEI-graphite interface. LiFOS channels the diffusion of Li$^+$ cations into the structure owing to its perfluorinated structure. F1110D combines the ligand effect of glyme groups and the properties of the fluorinated chain but acts less as a barrier because it does not have a polar head.

On the contrary, the fluorine spectra (F 1s) that consist of two peaks (at 687 eV attributed to LiPF$_6$ and at 685 eV assigned to LiF)[38] exhibit a significant increase in the form of LiF, which jumps from 4% to 37% and 25% in the presence of LiDS and F1110D, respectively (with and without LiF). The most common route of LiF formation stems from the decomposition of LiPF$_6$ in the presence of water.[31] Despite keeping the water content of LiDS to negligible levels, viz. < 10 ppm, we postulate that the LiF formation is accentuated in the presence of LiDS and F1110D due to mere amounts of water, highlighting the already known sensitivity of carbonate electrolytes to water.[39] What's more, the F 1s spectra point out equal amounts of LiPF$_6$ on each surface, signaling that full solvation of the salt irrespective of the additive. The Li 1s peak shows a binding energy of 55.6 eV (between 55.7 and 56.3 eV). From Figure 6, the Li 1 s peaks of Li$_2$CO$_3$, LiF and LiPF$_6$ are located at 55.5, 56.0 and 56.9 eV, respectively.

Starting from the reference electrolyte, there is a slight shift to the left with the addition of LiDS and F1110D that could imply the presence of LiF (i.e., high F content). In the presence of F1110D, 42% LiF and 24% carbonates are detected, while in presence of F1110D and LiF, 47% LiF and 15% carbonates are identified. The O 1s spectra show decreased peaks at 532.0 eV and 530.6 eV relative to the reference spectra. The main peak corresponds to ROCO$_2$Li species or lithium carbonate (Li$_2$CO$_3$). The other peaks correspond to surface oxygen species, for example, the decomposition products of solvents of the type PEO: H(CH$_2$CH$_2$O)$_n$R. Thus, the Li$_2$CO$_3$ amount is lower than that of the reference electrolyte due to the higher amounts of LiF. Knowing the importance of Li$_2$CO$_3$ in the quality of the SEI,[40] we can then explain why the galvanostatic cycling with Ref + LiDS alone was inferior to the reference and Ref + LiDS + LiF. Oxygen spectra indicates that the proportion of oxygen species at the surface, other than carbonates, is larger with F1110D similar to LiDS.

The phosphate content without and with LiF extends by 3.5 and 8.5%, respectively. The P 2p spectra comprise two unresolved doublets, 2p3/2 and 2p1/2, with a spin-orbit splitting of 0.85 eV. The first peak (termed phosphates) is evident at a binding energy of 134.5 eV and the PF$_6^-$ peak at 137.1 eV. For the first one, in the absence of the additives, the phosphate content was ca. 1.0%. Phosphates originate from the breakdown of LiPF$_6$, which in turn derives from a water level

increase in the electrolyte (in this case from LiDS and F1110D). A two-fold increase is noticed when LiDS is added to the reference electrolyte and a 1.5-fold increase in the presence of LiDS + LiF. The phosphates corresponding to PF$_6^-$ accounted for 8% of the reference electrolyte with LiDS and LiF. In the presence of LiDS alone, the PF$_6^-$ level reaches 6.4% suggesting that LIDs hinder the deposition of PF$_6^-$ and further dissociate the electrolyte. A different behavior is found for F1110D. Here, the LiF peak is larger than the (Li)PF$_6^-$ one. The amount of LiF extends to 43 and 47% (with and without LiF as an SEI component added to the electrolyte). Clearly, the action of F1110D, in this case, is to promote the LiF at the surface of the electrode.

Taking into account the XPS results, a mechanism of the action of the surfactants is proposed. The protection mechanism is effectively a barrier stemming from the lamellar organization that hinders salt deposition at the SEI by directing the diffusion of the Li$^+$ ions during the intercalation/deintercalation process as illustrated in Scheme 1.

LiFOS has both an ionic and fluorinated character, hence it has a dual action; that of retention and channelling of salts. In contrast, LiDS being an ionic surfactant but not fluorinated is effective in retaining polarized salts like LiF but not LiOH and Li$_2$O. The nonpolar F1110D bearing a long fluorinated and oxygenated chain can essentially act as a diffusion channel for the Li$^+$ cations towards the interface by the action of the oxygen as ligand and can retain the polar LiF far to SEI (Scheme 1).

The Nyquist plots gleaned from the graphite-Li half-cells in PC/EC/3DMC, 1 mol dm^{-3} LiPF$_6$ and the surfactants of Table 1 show a stable interfacial layer (i.e., graphite-electrolyte and lithium-electrolyte, 30–50 Ohm) in the presence of LiF in both lithiated (0.01 V vs. Li/Li$^+$, Figure 7a) and de-lithiated states (1.0 V vs. Li/Li$^+$, Figure 7b).

Surfactants significantly affect the interfaces, as shown by the highly distorted shapes of the spectra. It is very difficult to model them with standard equivalent circuits (commonly used for battery interfaces). We preferred to extract trends by comparing the spectra before (Figure 7a) and after (Figure 7b) lithiation, specifically looking at the resistances associated with the electrolyte/anode interface at high frequency domain, and the slope of the straight line for diffusion in the low-frequency regions. The semicircle intersection with the x-axis at high
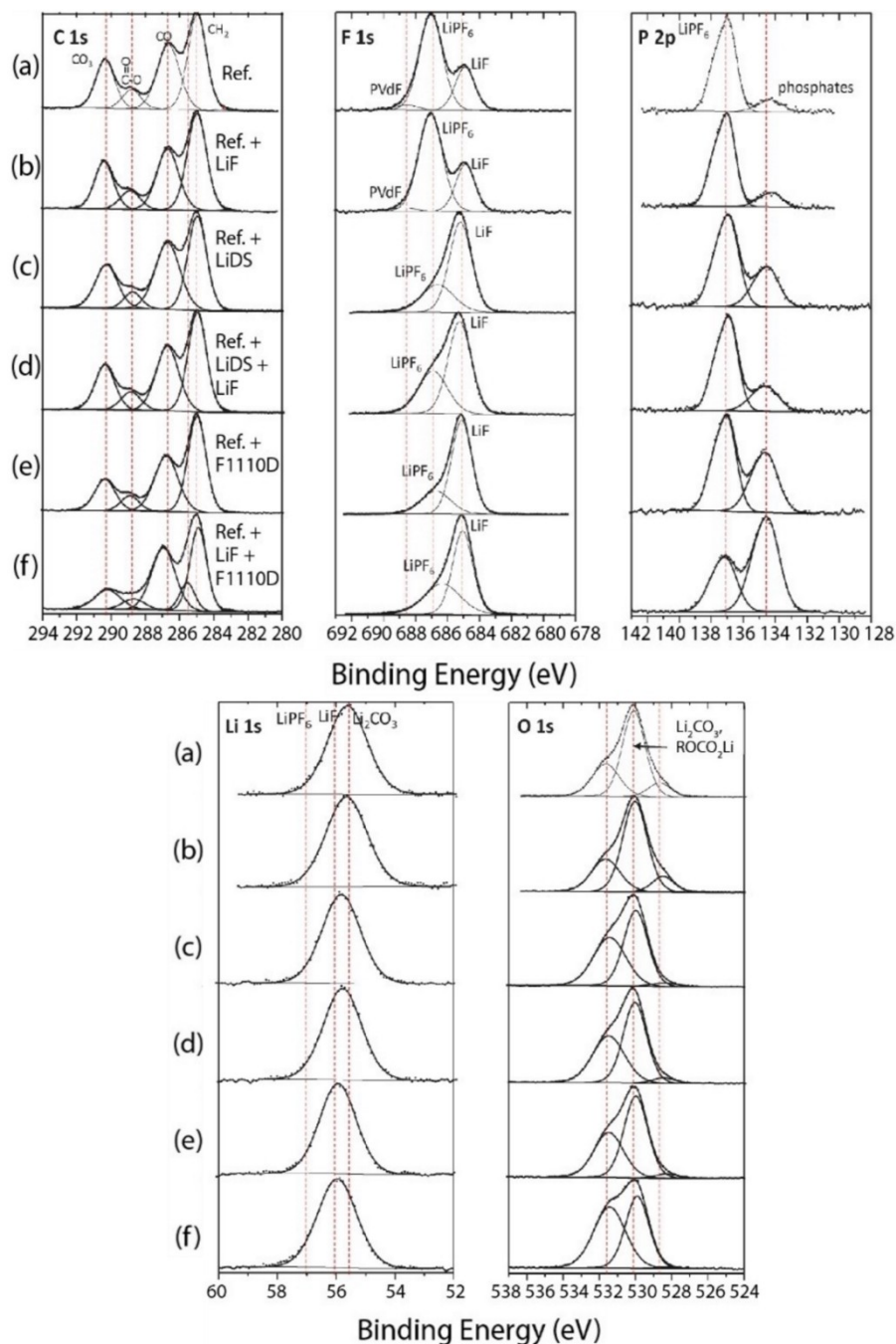
ChemElectroChem

Research Article
doi.org/10.1002/celc.202300102

Chemistry
Europe
European Chemical
Societies Publishing

Figure 6. XPS spectra (C 1s, F 1s, P 2p, Li 1s and O 1s) on graphite electrodes in the presence of (a) the reference electrolyte (Ref: EC/PC/3DMC + 1 mol dm^{-3} LiPF$_6$), (b) Ref + 0.3 mol dm^{-3} LiF, (c) Ref + LiDS, (d) Ref + LiDS + 0.3 mol dm^{-3} LiF, (e) Ref + F1110D and (f) Ref + F1110D + 0.3 mol dm^{-3} LiF. The composition of the surfactants is given in Table 1.

frequency denotes the series resistance, while information about charge-transfer resistance is given by the intersection at mid-frequency region. The slope of the straight line in the low-frequency region describes the Li-diffusion. At 1.0 V, the cell containing solely LiDS shows a distinct semi-circle where the charge transfer resistance reaches 15 ohms. The cells containing LiDS + LiF and LiDS + Li$_2$O exhibit a depressed semicircle, while the Nyquist plot with the cell containing LiDS + LiOH is a straight line (without any obvious semicircle) indicating an

exclusively capacitive charge storage mechanism with poor electronic conduction, rendering the suitability of this electrolyte unfeasible. At 0.01 V, the charge transfer resistance (R_{ct}) increased from 30 to 55 Ω when LiF was added to the carbonate electrolyte. The presence of Li$_2$O and LiOH further amplified R_{ct} (verified by the broadening of the semi-circle) leading to values that exceed 80 and 100 ohms. These observations confirm that polar LiF ($\mu = 6.33$ Debye) is better retained by anionic surfactants such as LiDS than for less polar
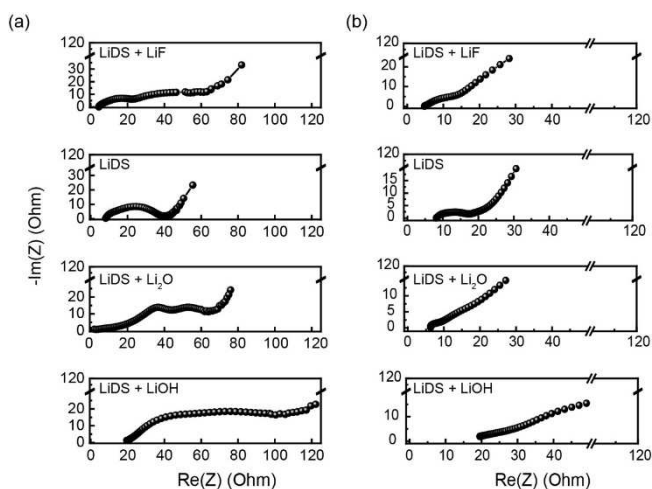
ChemElectroChem

Research Article
doi.org/10.1002/celc.202300102

**Chemistry
Europe**
European Chemical
Societies Publishing

Figure 7. Nyquist plots of graphite-Li half-cells in PC/EC/3DMC, 1 mol dm^{-3} LiPF$_6$, LiDS (at saturation) together with LiF, Li$_2$O and LiOH at (a) 0.01 (fully lithiated cell) and (b) 1.0 V (de-lithiated state).

salts such as LiOH ($\mu = 4.2$ Debye) and not polar ones such as Li$_2$O.[34]

Conclusion

The SEI layer is a passivating layer that acts as a barrier between the graphite anode and the electrolyte, but its formation inevitably generates harmful mineral byproducts (LiF, LiOH, Li$_2$O), whose surface precipitation over time can affect the overall performance of the cell. In this study, we demonstrate the suitability and protective action of three different surfactants, namely lithium dodecyl sulfate (LiDS), polyoxyethylene ether Forafac 1110D (LiF1110), and lithium perfluoro octanesulfonate Forafac 1185D (LiFOS), with respect to the SEI. By performing galvanostatic charge-discharge cycles over 15 cycles on a graphite anode, followed by XPS analysis and EIS measurements, we have highlighted different types of actions of these surfactants.The capacities obtained in the presence of surfactants alone in the first cycle are higher than that of the standard electrolyte at a C/10 rate. Furthermore,LiDS and F1110D counter the impact of LiF (a major SEI byproduct) reaching comparable specific capacities to the reference electrolyte. On the contrary, the effects of LiOH and Li$_2$O are not mitigated by LiDS and F1110D (i.e., drop in capacity) and are moderated by LiFOs. Higher LiF amounts do not influence the cycling capability of the graphite half-cell, signifying a modest SEI organization (i.e., good diffusion). The presence of LiDS is the most favorable to increase this capability.

The addition of SEI salts (e.g., LiF, LiOH, and Li$_2$O) reduces the discharge capacity in comparison to the reference electrolyte for all tested combinations, except for the F1110D+LiF and LiDS+LiF pairs. This consequently demonstrates the beneficial effect of these two surfactants, even in the presence of significant LiF deposits. The XPS results on the cycled graphite electrode highlight cell degradation resulting from the addition

of LiF without surfactants. The O 1 s spectra confirm the presence of oxygen species on the graphite surface due to the decomposition of carbonates (Li$_2$CO$_3$ or ROCO$_2$Li). Furthermore, the LiF signal varies depending on the surfactant (with or without the addition of LiF). LiDS is not detectable by the XPS machine, suggesting that it is not trapped within the SEI layer but contributes to its organization. Comparing the obtained results clearly shows that the chemical structure of surfactants plays a major role in their mode of action and emphasizes the beneficial effect of F1110D, which benefits from both its perfluorinated carbon chain and the presence of ether bonds.

Experimental Section

Materials

The reference electrolyte consists of a cyclic and linear carbonate mixture comprising PC, EC and DMC in a 1:1:3 ratio by weight (%w). The above solvents were purchased from Sigma-Aldrich and dried with desiccant bags (Distribio-Genecust). The lithium salt used as an ionic conductor is lithium hexafluorophosphate (LiPF$_6$, battery grade, >99.9% trace metal basis, Sigma Aldrich). The concentration of the salt was ca. 1 mol dm^{-3}. Lithium dodecyl sulfate (LiDS, >98.5%, Sigma Aldrich) is poorly soluble in the reference electrolyte, so it has been added at the saturation limit (see the following section for more details). Both the Forafac surfactant (F1110D) and lithium perfluoro octanesulfonate (LiFOS) concentrations were ca. 2.5×10^{-3} mol dm^{-3} (occupying <0.2% m of the total solution). The last two surfactants were provided by Arkema (France) in the form of aqueous solutions. The additives were dried under vacuum (viz., 1 mbar and 80°C for 10 h) to get rid of excess water. The SEI-related lithium salts namely lithium fluoride (LiF, ≥99.99% trace metals basis), lithium oxide (Li$_2$O, 97%, powder) and lithium hydroxide (LiOH, ≥98.0%) were purchased by Sigma Aldrich and used as received. The water levels of the formulated solution were measured by Karl Fisher coulometry and were found to be below 10 ppm. All the solutions were prepared in an Argon-filled glovebox (M-Braun).

Measurements

The solubility of LiDS was measured by atomic absorption spectroscopy (AAS) on a Thermo M Series FS 95 spectrometer (Thermo Scientific). The organic solvents were diluted in water (i.e., 10% dilution by volume). The air-acetylene burner was mounted on a premix-chamber atomizer. A lithium hollow-cathode source was employed for the AAS measurements, with a wavelength set to 670.8 nm. The sample aspiration rate was maintained at 0.8 mL min^{-1}. The spectrometer was pre-calibrated with a blank and a lithium perchlorate (LiCl, Sigma Aldrich) solution. The average standard derivation was 0.6%, for three sets of experiments. The AAS gives a peak that corresponds to the absorbance of the element analyzed, here lithium. The intensity of the peak is proportional to the concentration of the solution following the Beer–Lambert law (Figure S1) in Supporting Information.

Physicochemical and electrochemical testing

DSC was performed by a DSC 4000 (Perkin Helmer) between 60 and 150°C at a rate of 4°C min^{-1} under 20 Ml min^{-1} nitrogen flow. The samples were sealed into an aluminium cell. Prior to measurements, the solutions were heated to 100°C to limit the water that can be

ChemElectroChem

Research Article
doi.org/10.1002/celc.202300102

Chemistry Europe
European Chemical
Societies Publishing

adsorbed due to the use of perforated DSC capsules for these measurements. The surface tension of the formulated electrolytes is measured by the Du Noüy ring method[41] using a Krüss K100MK2 tensiometer equipped with a microbalance. The contact angle of the ternary carbonate electrolyte with and without the surfactants between different surfaces (i.e., polypropylene, polyethylene, and graphite) was measured by a contact angle tester (DSA10-Mk2, KRUSS Gmbh Germany) at room temperature through the sessile drop method. XPS measurements were carried out with a Kratos Axis Ultra spectrometer, using a focused monochromatized Al K$_\alpha$ radiation (h$v = 1486.6$ eV). The spectrometer was calibrated using the photoemission line Ag 3d5/2 (binding energy 368.3 eV). For the Ag 3d5/2 line, the full width at half-maximum (fwhm) was 0.58 eV under the recording conditions. The graphite electrodes analyzed by XPS were washed repeatedly with the carbonate electrolyte (EC/PC/3DMC) and dried overnight in an Argon glovebox at room temperature. The XPS spectrometer was directly connected to an argon dry box through a transfer chamber, to avoid moisture/air exposure to the samples. The analyzed area of the samples was 300×700 μm^2 and the analyzing depth was 5 nm of the surface of the electrode. The core peaks were analyzed using a non-linear Shirley-type background.[42]

Galvanostatic charge-discharge, CV and potentiostatic impedance spectroscopy (PEIS) measurements were performed in Teflon Swagelok system[43] with controlled pressure of 0.19 N mm^{-2} using a Multichannel Potentiostat VMP-3 (Biologic, France) piloted by an EC Lab V10.34 interface. The cyclic voltammetry tests were conducted by using a three-electrode configuration comprised Graphite disk (96.25% loading, $\emptyset = 10$ mm, from SAFT) as working electrode, platinum (purity $> 99.95\%$, $\emptyset = 10$ mm, Goodfellow) or Li foil (25 × 100 mm, thickness: 0.6 mm, Sigma Aldrich) as a counter electrode and a Li ribbon (Sigma Aldrich) as a reference electrode was used, inserted between two polypropylene separators (thickness: 25 μm, pore diameter: 0.2–0.5 μm, Celgard). For galvanostatic charge-discharge of the graphite-Li metal half-cell, the cut-off voltage was set to 0.02 mV vs. Li/Li$^+$ for discharge (i.e., lithiation) and 1.0 V vs. Li/Li$^+$ for charge (i.e., delithiation). A 1C rate corresponds to 372 mA g^{-1} on the weight basis of graphite. PEIS was conducted between 0.1 MHz and 10 mHz (ten points per decade) at open-circuit voltage with an oscillating amplitude fixed at 10 mV. The quality of the EIS spectra highly affected by surfactant at interface was validated through the Kramers-Kronig test but no modeled par equivalent circuit.

Conflict of Interests

The authors declare no conflict of interest.

Data Availability Statement

The data that support the findings of this study are available in the supplementary material of this article.

[1] a) G. Nikiforidis, M. Raghibi, A. Sayegh, M. Anouti, *J. Phys. Chem. Lett.* **2021**, *12*, 1911–1917; b) J. Asenbauer, T. Eisenmann, M. Kuenzel, A. Kazzazi, Z. Chen, D. Bresser, *Sustain. Energy Fuels* **2020**, *4*, 5387–5416.

[2] Y. Pei, Q. Chen, M. Wang, P. Zhang, Q. Ren, J. Qin, P. Xiao, L. Song, Y. Chen, W. Yin, X. Tong, L. Zhen, P. Wang, C.-Y. Xu, *Nat. Commun.* **2022**, *13*, 6158.

[3] a) S. K. Heiskanen, J. Kim, B. L. Lucht, *Joule* **2019**, *3*, 2322–2333; b) Y. Li, M. Liu, X. Feng, Y. Li, F. Wu, Y. Bai, C. Wu, *ACS Energy Lett.* **2021**, *6*, 3307–3320.

[4] K. Ushirogata, K. Sodeyama, Y. Okuno, Y. Tateyama, *J. Am. Chem. Soc.* **2013**, *135*, 11967–11974.

[5] a) F. Chrétien, J. Jones, C. Damas, D. Lemordant, P. Willmann, M. Anouti, *J. Power Sources* **2014**, *248*, 969–977; b) K. Tasaki, A. Goldberg, J.-J. Lian, M. Walker, A. Timmons, S. J. Harris, *J. Electrochem. Soc.* **2009**, *156*, A1019.

[6] L. Wang, A. Menakath, F. Han, Y. Wang, P. Y. Zavalij, K. J. Gaskell, O. Borodin, D. Iuga, S. P. Brown, C. Wang, K. Xu, B. W. Eichhorn, *Nat. Chem.* **2019**, *11*, 789–796.

[7] Y. S. Meng, V. Srinivasan, K. Xu, *Science* **2022**, *378*, eabq3750.

[8] a) A. Baig, J. Fox, R. Young, Z. Wang, J. Hsu, W. Higuchi, A. Chhettry, H. Zhuang, M. Otsuka, *Calcif. Tissue Int.* **1999**, *64*, 437–449; b) J. Jones, M. Anouti, M. Caillon-Caravanier, P. Willmann, P.-Y. Sizaret, D. Lemordant, *Fluid Phase Equilib.* **2011**, *305*, 121–126.

[9] a) M. Herstedt, A. M. Andersson, H. Rensmo, H. Siegbahn, K. Edström, *Electrochim. Acta* **2004**, *49*, 4939–4947; b) J. Tan, J. Matz, P. Dong, J. Shen, M. Ye, *Adv. Energy Mater.* **2021**, *11*, 2100046; c) S. Shi, Y. Qi, H. Li, L. G. Hector Jr, *J. Phys. Chem. C* **2013**, *117*, 8579–8593.

[10] K. N. Wood, G. Teeter, *ACS Appl. Energ. Mater.* **2018**, *1*, 4493–4504.

[11] K. Huang, S. Bi, B. Kurt, C. Xu, L. Wu, Z. Li, G. Feng, X. Zhang, *Angew. Chem.* **2021**, *133*, 19381–19389; *Angew. Chem. Int. Ed.* **2021**, *60*, 19232–19240.

[12] H.-L. Tsai, C.-T. Hsieh, J. Li, Y. A. Gandomi, *Electrochim. Acta* **2018**, *273*, 200–207.

[13] S. S. Zhang, *J. Power Sources* **2006**, *162*, 1379–1394.

[14] a) H. Dai, K. Xi, X. Liu, C. Lai, S. Zhang, *J. Am. Chem. Soc.* **2018**, *140*, 17515–17521; b) Y. Cao, S. Yang, Y. Li, J. Shi, *Aggregate* **2021**, *2*, e49.

[15] M. Qin, Z. Zeng, X. Liu, Y. Wu, R. He, W. Zhong, S. Cheng, J. Xie, *Adv. Sci.* **2023**, *10*, 2206648.

[16] A. Tudela Ribes, P. Beaunier, P. Willmann, D. Lemordant, *J. Power Sources* **1996**, *58*, 189–195.

[17] N. von Aspern, G.-V. Röschenthaler, M. Winter, I. Cekic-Laskovic, *Angew. Chem. Int. Ed.* **2019**, *58*, 15978–16000; *Angew. Chem.* **2019**, *131*, 16124–16147.

[18] M. M. Singer, R. S. Tjeerdema, in *Reviews of Environmental Contamination and Toxicology* (Ed.: G. W. Ware), Springer New York, New York, NY, **1993**, pp. 95–149.

[19] J. Hao, J. Long, B. Li, X. Li, S. Zhang, F. Yang, X. Zeng, Z. Yang, W. K. Pang, Z. Guo, *Adv. Funct. Mater.* **2019**, *29*, 1903605.

[20] S. Kondou, A. Morinaga, K. Hashimoto, Y. Katayama, K. Dokko, M. Watanabe, K. Ueno, *ChemElectroChem* **2022**, *9*, e202200870.

[21] J. Huang, J. Liu, J. He, M. Wu, S. Qi, H. Wang, F. Li, J. Ma, *Angew. Chem. Int. Ed.* **2021**, *60*, 20717–20722; *Angew. Chem.* **2021**, *133*, 20885–20890.

[22] Y. Nishikami, T. Konishi, R. Omoda, Y. Aihara, K. Oyaizu, H. Nishide, *J. Mater. Chem. A* **2015**, *3*, 10845–10850.

[23] J. G. Riess, *Curr. Opin. Colloid Interface Sci.* **2009**, *14*, 294–304.

[24] X. Ji, K. T. Lee, L. F. Nazar, *Nat. Mater.* **2009**, *8*, 500–506.

[25] E. P. Roth, *ECS Trans.* **2008**, *11*, 19.

[26] K. Xu, *Chem. Rev.* **2004**, *104*, 4303–4418.

[27] J. Tadano, *Vol. US20090061313A1*, US20090061313A1, US, **2007**.

[28] a) G. Nikiforidis, M. Anouti, *Batteries & Supercaps* **2021**, *4*, 1708–1719; b) Ch. L. Berhaut, D. Lemordant, P. Porion, L. Timperman, G. Schmidt, M. Anouti, *RSC Adv.* **2019**, *9*, 4599–4608; c) C. L. Berhaut, P. Porion, L. Timperman, G. Schmidt, D. Lemordant, M. Anouti, *Electrochim. Acta* **2015**, *180*, 778–787.

[29] G. Nikiforidis, J. Pires, S. Phadke, M. Anouti, *ChemElectroChem* **2022**, *9*, e202200571.

[30] L. Seidl, S. Martens, J. Ma, U. Stimming, O. Schneider, *Nanoscale* **2016**, *8*, 14004–14014.

[31] M. Pierpaoli, M. Szopińska, B. K. Wilk, M. Sobaszek, A. Łuczkiewicz, R. Bogdanowicz, S. Fudala-Książek, *J. Hazard. Mater.* **2021**, *403*, 123606.

[32] Y. Bencherifi, B. Larhrib, A. Sayegh, G. Nikiforidis, M. Anouti, *J. Appl. Electrochem.* **2021**, *51*, 1651–1664.

[33] A. Andersson, K. Edström, *J. Electrochem. Soc.* **2001**, *148*, A1100.

[34] J. Jones, M. Anouti, M. Caillon-Caravanier, P. Willmann, D. Lemordant, *Fluid Phase Equilib.* **2009**, *285*, 62–68.

[35] H. Wu, H. Jia, C. Wang, J. G. Zhang, W. Xu, *Adv. Energy Mater.* **2021**, *11*, 2003092.

[36] X. Gong, Y. Zheng, J. Zheng, S. Cao, H. Wen, B. Lin, Y. Sun, *ChemElectroChem* **2020**, *7*, 1465–1472.

[37] S. Obata, H. Tanaka, K. Saiki, *Carbon* **2013**, *55*, 126–132.

[38] T. Liu, A. Garsuch, F. Chesneau, B. L. Lucht, *J. Power Sources* **2014**, *269*, 920–926.

[39] a) A. Guéguen, D. Streich, M. He, M. Mendez, F. F. Chesneau, P. Novák, E. J. Berg, *J. Electrochem. Soc.* **2016**, *163*, A1095; b) I. A. Profatilova, S.-S. Kim, N.-S. Choi, *Electrochim. Acta* **2009**, *54*, 4445–4450.

[40] a) D. Wu, J. He, J. Liu, M. Wu, S. Qi, H. Wang, J. Huang, F. Li, D. Tang, J. Ma, *Adv. Energy Mater.* **2022**, *12*, 2200337; b) Y. Yang, Z. Fang, Y. Yin, Y. Cao, Y. Wang, X. Dong, Y. Xia, *Angew. Chem.* **2022**, *134*, e202208345; c) S. Klein, P. Harte, J. Henschel, P. Bärmann, K. Borzutzki, T. Beuse, S. van Wickeren, B. Heidrich, J. Kasnatscheew, S. Nowak, *Adv. Energy Mater.* **2021**, *11*, 2003756.

[41] B.-B. Lee, E.-S. Chan, P. Ravindra, T. A. Khan, *Polym. Bull.* **2012**, *69*, 471–489.

[42] J. Pires, A. Castets, L. Timperman, J. Santos-Peña, E. Dumont, S. Levasseur, C. Tessier, R. Dedryvère, M. Anouti, *J. Power Sources* **2015**, *296*, 413–425.

[43] J. Chidiac, G. Nikiforidis, L. Timperman, M. Anouti, *ChemPhysChem* **2022**, *23*, e202200224.

RESEARCH ARTICLE

Surfactant protection: The protective roles of three surfactants added to the electrolyte in the formation of the solid electrolyte interphase (SEI) layer on the graphite anode are compared and analyzed. Through electrochemical testing and surface characterization, it was observed that each surfactant had a distinct impact on the cycling behavior and performance of the cells.
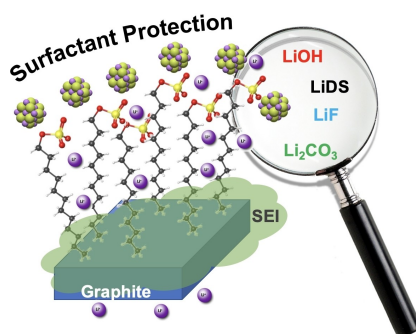
Dr. F. Chrétien, Dr. G. Nikiforidis, Dr. C. Damas, Prof. M. Anouti*

1 – 12

Lithium-Ion Batteries Containing Surfactants for the Protection of Graphite Anode against the Passivation Layer Byproducts